LBL-15535 c.2
Preprint

Lawrence Berkeley Laboratory

UNIVERSITY OF CALIFORNIA

RECEIVED
LAWRENCE
BERKELEY LABORATORY
JUN 8 1983
LIBRARY AND
DOCUMENTS SECTION

ENERGY & ENVIRONMENT DIVISION

Submitted to Applied Physics A

PHOTOTHERMAL DISPLACEMENT SPECTROSCOPY:
A NEW OPTICAL PROBE FOR SOLIDS AND SURFACES

M. A. Olmstead, N. M. Amer, S. Kohn,
D. Fournier and A. C. Boccara

December 1982

TWO-WEEK LOAN COPY

This is a Library Circulating Copy which may be borrowed for two weeks. For a personal retention copy, call Tech. Info. Division, Ext. 6782.

ENERGY
AND ENVIRONMENT
DIVISION

Prepared for the U.S. Department of Energy under Contract DE-AC03-76SF00098

LBL-15535 c.2

DISCLAIMER

This document was prepared as an account of work sponsored by the United States Government. While this document is believed to contain correct information, neither the United States Government nor any agency thereof, nor the Regents of the University of California, nor any of their employees, makes any warranty, express or implied, or assumes any legal responsibility for the accuracy, completeness, or usefulness of any information, apparatus, product, or process disclosed, or represents that its use would not infringe privately owned rights. Reference herein to any specific commercial product, process, or service by its trade name, trademark, manufacturer, or otherwise, does not necessarily constitute or imply its endorsement, recommendation, or favoring by the United States Government or any agency thereof, or the Regents of the University of California. The views and opinions of authors expressed herein do not necessarily state or reflect those of the United States Government or any agency thereof or the Regents of the University of California.

PHOTOTHERMAL DISPLACEMENT SPECTROSCOPY: A NEW OPTICAL PROBE FOR SOLIDS AND SURFACES*

Marjorie A. Olmstead, Nabil M. Amer, and Stanley Kohn+

Applied Physics and Laser Spectroscopy Group
Lawrence Berkeley Laboratory
University of California
Berkeley, CA 94720 U.S.A.

and

Daniele Fournier and A. Claude Boccara

Laboratoire d'Optique Physique
Ecole Supérieure de Physique et de Chimie
10 rue Vauquelin, 75231 Paris Cedex 05, France

Abstract

We present a sensitive technique for determining the optical and thermal properties of solids, surfaces and thin films. This technique, photothermal displacement spectroscopy, is based on the detection of the thermal expansion of a sample upon absorption of electromagnetic radiation. The technique is well suited for *in situ* ultrahigh vacuum studies and for experiments where wide temperature ranges are required. We show that surface and bulk optical absorption can be readily distinguished and that absorptions of $\alpha L = 10^{-6}$/Watt can be measured. The theoretical basis of the signal generation is given, and excellent experimental and theoretical agreement is demonstrated. The implications of our findings to imaging and microscopy are discussed.

P.A.C.S.: 73; 78; 65

* Preliminary results were presented at the American Physical Society March Meeting, Dallas, TX, 1982, Bull. Amer. Phys. Soc., 27, 227, (1982).

+ Current Address: Aerospace Corporation, Los Angeles, CA 90009 U.S.A.

PHOTOTHERMAL DISPLACEMENT SPECTROSCOPY: A NEW OPTICAL PROBE FOR SOLIDS AND SURFACES

I. INTRODUCTION

Increasing interest in the properties of surfaces and interfaces and the continuing need for *in situ* characterization of thin films require the development of new, sensitive, and reliable probes of the optical properties of these materials. Although a variety of traditional optical methods have been employed to study the electronic surface states in solids [1, 2] and the optical absorption in thin films [3], implementation of these methods can be cumbersome and complicated in the difficult environments often required for such studies. Also, elaborate data analysis is frequently required to obtain the desired optical information.

We present a sensitive photothermal technique [4] which directly and simultaneously measures the optical and thermal parameters of solids. The underlying physical principle of photothermal displacement spectroscopy is the buckling and displacement of an illuminated surface due to the thermal expansion of a sample as it is heated by the absorption of electromagnetic radiation. This optically induced surface displacement is exploited to determine quantitatively the optical and thermal parameters of materials.

Important features of photothermal displacement spectroscopy include the ability to distinguish between surface and bulk properties, the absence of any electrical or mechanical contact with the sample, and the ease of application to the study of a wide variety of materials in difficult environments. For example, this technique can be readily

implemented *in vacuo* during the deposition of superlattice structures, thin films, or adsorbates. The technique is particularly well suited for microscopy, imaging and non-destructive depth profiling, being a more localized probe than other photothermal techniques. Furthermore, photothermal displacement spectroscopy should prove useful for the investigation of non-radiative processes. Among the advantageous properties of this technique for measuring the optical absorption coefficient, α, of a material is the direct detection of the heat deposited by the absorption of light. This yields a signal which is linear over a large range of α and insensitive to scattering of the incident beam. It also eliminates the need for a photodetector sensitive in the wavelength region being investigated. These characteristics all combine to make photothermal displacement spectroscopy particularly suited for the study of solid surfaces, interfaces, and thin films.

In Section II of this paper we present the theoretical framework of photothermal displacement spectroscopy. In Section III we describe three approaches to performing this technique: beam deflection; interferometry; and attenuated total reflection. The signal sensitivity and optimization criteria are also discussed. Experimental results are presented and compared with the theoretical predictions in Section IV. A detailed discussion of our findings is given in Section V , with particular emphasis given to the differentiation of surface and bulk information and the implication of our results for microscopy and imaging.

II. THEORY OF PHOTOTHERMAL DISPLACEMENT

All three experimental schemes described below are based on detecting the displacement of the sample surface produced by the absorption of energy from a light beam incident on the sample. The sample will be heated as the optically excited electrons decay non-radiatively, and it will expand as the temperature rises.

A crude expression for the displacement of the surface is:

$$h = \alpha_{th} T L_{eff} \tag{1}$$

where α_{th} is the thermal expansion coefficient, and T is the average rise in temperature over an effective length L_{eff}. The temperature rise is given by T ~ (absorbed energy/volume)/(heat capacity). If the light is intensity modulated at frequency f, then the incident energy per cycle (of which some fraction is absorbed) is given by the product of the incident power and the time it is incident on the sample, or (Power/2f) for square wave modulation. The surface displacement is approximately given by:

$$h = \alpha_{th} \beta P/(2A\ f p C) \tag{2}$$

where β = fraction of light absorbed
P = incident power
A = heated area
p = mass density
and C = heat capacity/gram

The inverse proportionality to the modulation frequency is valid in the limit that the thermal diffusion length of the material is much less than the diameter of the pump beam on the sample. The thermal diffusion length is the distance over which the magnitude of a planar harmonic thermal wave decays exponentially to 1/e of its initial value and its

phase changes by one radian. It is given by

$$L_{th} = (K_{th}/\pi f p C)^{1/2} = (\lambda/\pi f)^{1/2} \quad (3)$$

where K_{th} = thermal conductivity,
p = mass density
C = heat capacity per gram
f = frequency of the thermal wave
and $\lambda = K_{th}/pC$ = thermal diffusivity.

If L_{th} is greater than the pump beam waist on the sample, the size of the heated area, A, will depend on the modulation frequency through equation 3.

A rigorous calculation of the surface displacement involves solving the Navier-Stokes equation for a slab, subject to the condition that there is no normal component to the stress at the boundaries of the slab:

$$(1-2\nu)\ \nabla^2 u + \nabla(\nabla\cdot u) = 2(1+\nu)\alpha_{th}\ \nabla T \quad (4)$$

where u = displacement vector
ν = Poisson ratio
T = change in temperature from equilibrium value
and α_{th} = thermal expansion coefficient.

The temperature distribution is assumed to be unaffected by the expansion and is found by solving the heat equation with a source term of a Gaussian beam decaying exponentially by optical absorption:

$$K_{th}\ \nabla^2 T - p C(\partial/\partial t)T = -Q(r,t) \quad (5)$$

where K_{th} = thermal conductivity

$$Q(r,t) = (P\alpha/2\pi a^2)\exp(-r^2/a^2)\exp(-\alpha z)\cos(\omega t)$$

P = pump beam power
a = 1/e radius of the Gaussian pump beam
$\omega = 2\pi f$ = (angular) frequency of modulation
and α = optical absorption coefficient.

Details of the calculation are given in the Appendix.

In typical performance of photothermal displacement spectroscopy the measured quantity is proportional to the slope of the photoinduced displacement at the sample surface. The solution of the thermoelastic equations (equations 4 and 5) for this quantity yields:

$$\frac{\partial \mu_z}{\partial r}(r,0) = -\frac{\alpha_{th}\alpha P(1+\nu)}{16\pi K_{th}(1-\nu)}\left[\int_0^\infty \frac{\Delta^2 d\Delta J_1(\Delta r/L)\exp(-\Delta^2 a^2/4L^2)}{\sinh\Delta[(\alpha L)^2 - S^2]} \times \{R(\alpha L) + C_1 R(-S) + C_2 R(S)\} + C.C.\right] \quad (6)$$

where $R(x) = \left[\frac{e^x - e^\Delta}{x-\Delta} - \frac{e^x - e^{-\Delta}}{x+\Delta}\right] + B_1\left[\frac{e^{x+\Delta/2} - e^{-\Delta/2}}{x+\Delta} + \frac{e^{x-\Delta/2} - e^{\Delta/2}}{x-\Delta}\right] + B_2\left[\frac{e^{x+\Delta/2} - e^{-\Delta/2}}{x+\Delta} - \frac{e^{x-\Delta/2} - e^{\Delta/2}}{x-\Delta}\right]$

$C_{1,2} = (\alpha L/S)[(\exp(-\alpha L) - \exp(\pm S))/2\sinh(S)]$

$B_1 = -\sinh(\Delta)[\Delta - (1 - 2\nu)\sinh(\Delta)]/[\Delta + \sinh(\Delta)]$

$B_2 = \cosh(\Delta)[\Delta + (1 - 2\nu)\sinh(\Delta)]/[\Delta - \sinh(\Delta)]$

$S^2 = \Delta^2 + i(L^2/2L_{th}^2)$

L = sample thickness

and L_{th} = thermal length

This is equivalent to equation A12 in the Appendix.

Some general statements can be made about the form of equation 6. The signal is directly proportional to the pump beam power and the thermal expansion coefficient of the sample. Although the absorption coefficient appears many different places in the integral, the signal is linear in α when $\alpha L_{th} \ll 1$. The inverse proportionality to the thermal conductivity of the sample in the prefactor is the only time the thermal

conductivity appears without the density, heat capacity and modulation frequency. Within the integral, these factors always occur together as the thermal diffusion length, the parameter which describes both the decay and wavelength of a thermal wave. The result is fairly insensitive to the value of ν, the Poisson ratio, for typical values of the parameter. In all of the calculations presented here, ν was taken to be 0.25. The radius of the pump beam, a, occurs only in the Gaussian envelope under the integral. If the ratio of the radius to the sample thickness, a/L, is small, the Gaussian decays slowly, and the Bessel function has more time to oscillate. Care must be taken in choice of a numerical integrating routine to account for this. The three terms in the curly brackets are derived from the three exponential terms in the temperature distribution: direct heating from the optical absorption and the forward and reverse thermal waves. Within R(x), the three terms are derived from the particular solution to the Navier-Stokes equation and the symmetric and anti-symmetric parts of the homogeneous solution needed to meet the stress free boundary conditions. The theoretical curves in Figs. 2,4, and 5 were calculated using equation 6.

The photothermal displacement is a very small perturbation of the sample surface. For example, consider one milliwatt of power focussed to a radius of 75 microns and modulated at 320 Hz, fully absorbed at the surface of a 0.33 cm thick silicon sample. The maximum slope calculated from (6) is 1.4×10^{-8}, and the maximum displacement is 3.2×10^{-2} Å (obtained by numerical integration of (6) over r). As we show in Section III, such small displacements can be readily detected.

III. EXPERIMENTAL CONSIDERATIONS

We describe below three schemes for measuring the magnitude and phase of the optically induced displacement. The first measures the slope of the displacement while the last two detect the displacement itself. For a given pump beam profile, an increase in the magnitude of a surface absorption should change the overall magnitude of the photothermal displacement, but not the shape. Thus a measurement of the slope of the photoinduced displacement should be equivalent to a measurement of its height. The slope and height of the displacement have somewhat different dependences on the modulation frequency of the pump beam, and the slope is the more local probe of the optical absorption when the pump beam waist is smaller than the thermal diffusion length. In general, however, the slope and height yield similar information for both surface and bulk absorptions. For a Gaussian beam, as is usually the case for laser excitation, calculation of the slope, or radial derivative of the normal surface displacement, is straightforward (see Appendix).

A. EXPERIMENTAL CONFIGURATION

1. Beam Deflection Scheme. Details of this detection scheme are given in Fig. 1a. The sample is irradiated by the focussed pump beam, and a weak probe beam, typically a HeNe laser, is reflected from the sample. As the pump beam intensity is modulated, the photoinduced displacement rises and falls, and the probe beam is reflected at a different angle depending on the slope (du_z/dr) of the displacement at the point (r_0) where the probe is reflected from the sample (see Fig. 1b). The deflection of the probe beam is detected by a position sensitive

photodiode and the output is amplified by a phase-sensitive lock-in amplifier referenced to the mechanical chopper.

The beam deflection signal at the position sensor is given by

$$S = \{2D(du_z/dr(r_0)) + 2u_z(r_0)\sin\theta + \text{smaller terms}\}\gamma \qquad (7)$$

where D is the distance from the sample to the position sensor, u_z is the surface displacement, θ is the angle of incidence of the probe beam and γ is the position sensor sensitivity (Volts/cm). The first term in equation 7 is the deflection by the slope of the displacement. The second term is the small deflection of the probe beam by the vertical surface displacement, and is smaller than the first term by a factor of approximately D/a where a is the pump beam radius. This is typically about 5000. Higher order terms are due to the slight displacement of the position (r_0) where the probe beam falls onto the sample when the displacement is present from that when it is absent. It is a very good approximation to assume that the signal is due only to the first term and thus is directly proportional to the slope of the surface displacement.

2. Interferometric Scheme. In this detection scheme (see Fig. 1c) the sample serves as one arm of a conventional Michaelson interferometer. The mirror used in the other arm is mounted on a piezoelectric transducer (pzt) for signal stabilization. The intensity of the pump beam incident on the sample is again modulated causing the surface displacement to rise and fall with (angular) frequency ω_1, and a small oscillation is applied to the mirror through the pzt at a frequency ω_2. The total path difference between the two arms of the interferometer for the probe laser is given by

$$2\delta = 2(\delta_0 + \delta_1\cos(\omega_1 t) + \delta_2\cos(\omega_2 t+\phi)) \tag{8}$$

where δ_0= static path difference (controlled by DC voltage to the pzt)

δ_1= amplitude of photothermally induced displacement on sample

and δ_2= amplitude of mirror oscillation (controlled by AC voltage to the pzt)

The signal at the photodiode has the form

$$S = S_0\cos(4\pi\delta/\lambda) + \text{constant} \tag{9}$$

where λ = the wavelength of the probe laser. Defining

$$\xi_i = 4\pi\delta_i/\lambda\ , \tag{10}$$

inserting equation 8 into equation 9, and expanding the nested trigonometric functions in terms of Bessel functions, yields, among others, a term at the pump beam modulation frequency,

$$S(\omega_1) = -S_0\sin\xi_0 J_0(\xi_2)J_1(\xi_1)\cos(\omega_1 t). \tag{11}$$

For small ξ_1 and ξ_2 (δ_1 and δ_2 < 75 Å for 1% accuracy with HeNe probe) this term is linear in the surface displacement:

$$S(\omega_1) \cong -S_0\sin\xi_0(2\pi/\lambda)\delta_1\cos(\omega_1 t). \tag{12}$$

When $|\sin\xi_0|$ is at its maximum value of unity, the $\cos\xi_0$ is zero and the term in the photodiode signal at twice the pzt modulation frequency is then zero:

$$S(2\omega_2) = S_0\cos\xi_0 J_0(\xi_1)J_2(\xi_2)\cos(2\omega_2 t) = 0. \tag{13}$$

This condition is established by a servo loop consisting of a lock-in amplifier at $2\omega_2$ and an integrator used to control the DC voltage on the reference mirror pzt. Active stabilization of the interferometer is essential to eliminate signal drifts resulting from thermal fluctuations

and acoustic disturbances in the interferometer elements.

The prefactor, S_0, depends on the intensity of the probe beam and the interferometer alignment. Experimentally, it can be determined as one half of the peak to peak change in S as δ is swept through a distance of $\lambda/4$ by adjusting the DC voltage to the pzt. This removes the alignment and photodiode sensitivity from the determination of the height of the displacement. A similar inherent calibration cannot be made for the beam deflection method, although the beam deflection signal can be calibrated using the position sensor sensitivity (Volts/cm), an easily measured quantity.

3. Attenuated total reflection scheme. In this approach, the photothermal displacement is measured in an attenuated total reflection (ATR) geometry, where a transparent prism is placed in close proximity to the sample surface (Fig. 1d). The width of the gap between the sample and prism is modulated as the photoinduced displacement rises and falls. A probe beam of light internally reflected by the prism will couple some of its energy into the sample via the evanescent field that exists in the gap. Since the evanescent field decays exponentially in the gap as $\exp(-2k_g d)$, where d is the gap width and $k_g = (2\pi/\lambda)(n^2\sin^2\theta - 1)^{1/2}$, small changes in the gap width, d, produce large changes in the amount of the probe beam that is coupled into the sample, and therefore a change in the intensity of the reflected probe beam. A calculation of the probe beam transmission through the prism yields

$$T = \left| \frac{\gamma(k_p + \varepsilon_p k_g) + \exp(-2k_g d)(k_p - \varepsilon_p k_g)}{\gamma(k_p - \varepsilon_p k_g) + \exp(-2k_g d)(k_p + \varepsilon_p k_g)} \right|^2 \qquad (14)$$

where p,g and s denote prism, gap and sample, respectively

$$\gamma = (\varepsilon_s k_g - k_s)/(\varepsilon_s k_g + k_s)$$

ε = dielectric constant

$$k_{p,g,s} = (k_0^2\, \varepsilon_{p,g,s} - k_{\parallel}^2)^{1/2}$$

$k_0 = 2\pi/\lambda$ of the probe beam

and $k_{\parallel}$ = component of probe beam wave vector, k, parallel to interface.

The sensitivity of this method is given by the derivative of the transmission with respect to the gap distance, or $\partial T/\partial d$. For a well chosen gap spacing this method can have usable sensitivity. Because the ATR method requires careful spacing between the prism and the sample, and because it has lower sensitivity than the beam deflection and interferometric methods, it might not generally be as useful as the other two methods in surface experiments.

B. SENSITIVITY AND OPTIMIZATION

The interferometric and beam deflection schemes have comparable sensitivities under normal laboratory conditions. The measured noise level in the interferometer is equivalent to an effective surface displacement of about 4×10^{-3} Å/$\sqrt{\text{Hz}}$; in the beam deflection configuration the noise level is equivalent to an effective slope of about $1\times10^{-9}/\sqrt{\text{Hz}}$. For a 0.33 cm thick silicon sample with the pump beam focussed for a Gaussian beam 1/e radius of 75 microns and modulated at 320 Hz (300 micron thermal length), the interferometer noise level is equivalent to about 125 microwatts of power absorbed at the sample surface, and the beam deflection noise level is equivalent to about 70 microwatts of absorbed power. For a given pump beam radius and thermal diffusion length, the signal on different samples is proportional to the thermal

expansion coefficient, and inversely proportional to the thermal conductivity. For silicon, copper and fused silica, the ratio α_{th}/K_{th} takes on the relative values of 1, 2.37 and 20.5, respectively. Filter glass has a higher thermal expansion coefficient and a lower thermal conductivity than fused silica, and would thus have an even higher sensitivity, or less than 1 microwatt deposited in a thin film at the surface. For the attenuated total reflection detection scheme, the probe beam transmission changes on the order of 10^{-3}/Angström of displacement for a gap spacing of order 100 Å between a glass prism and a sample of index 2.0.

The inherent sensitivity of photothermal displacement is larger for a surface absorption than for an equivalent amount of power absorbed throughout the sample. This is still true when the effective length of the sample is taken to be the thermal diffusion length. For example, consider a beam deflection measurement on a silicon sample 0.33 cm thick with a pump beam 1/e radius of 75 microns and a modulation frequency of 320 Hz. (L_{th} = 300 microns). The predicted slope for an absorption coefficient of $10^7 cm^{-1}$, where all of the light is absorbed in the first few tens of Angströms, is 1.4×10^{-8} per incident milliwatt of power. The predicted signal for an absorption coefficient of $10^{-3} cm^{-1}$ is 2.2×10^{-13} per incident milliwatt. With this uniform absorption, the signal saturates when the sample is longer than a few thermal lengths, (see Eq. 16). The ratio of the surface to bulk absorption signals per incident milliwatt is 6.4×10^4, equal to the ratio of power absorbed in about the first half of a thermal length.

There are a number of ways to optimize the signal to noise ratio of the photothermal displacement signal. The signal magnitude can be maximized by tighter focussing of the pump and probe beams, although the probe beam should remain the smaller of the two for ease of data interpretation. In the beam deflection scheme, the signal increases with the distance between the sample and the position sensor. The probe beam diameter, however, must remain smaller than the active element in the position sensor as the beam diverges after being focussed on the sample. Also, longer beam paths are more sensitive to disturbance. Phase sensitive detection referenced to the pump beam modulation is essential. This increases the signal to noise ratio considerably and enables the extraction of information from the phase of the signal.

The signal, in general, decreases with the modulation frequency of the pump beam. However, when the thermal length is larger than the pump beam waist, the decay is very slow, especially for a thermally thin or optically thick sample. Often, the noise is lower at higher modulation frequencies, and it may be advantageous to work at kilohertz frequencies when obtaining optical information about a sample with high thermal conductivity. It is necessary to vary the frequency when obtaining thermal information, as will be discussed in Section V. Occasionally, there may be resonances in the sample holder or optical bench, or interference from other electrical equipment which should also be considered in the choice of modulation frequency.

The sample and any other components which reflect the probe beam should be mounted securely, but with sufficient degrees of freedom to assist in the alignment. It is helpful to work on a vibrationally iso-

lated table or optical bench and to shield the beam paths from air currents, especially in the interferometric detection scheme. We find, however, the pointing and intensity fluctuations of the probe beam to be the dominant factor in setting the limits of our sensitivity.

The interferometer is quite sensitive to small changes in the optical path and long term stability can be a problem as it is difficult to obtain the same alignment reproducibly. In the beam deflection (BD) configuration, the sample can be replaced or one of the beams misaligned, and the alignment can be recovered readily if care is taken not to move other elements of the experimental configuration. In the case of laser excitation, it is always easier to use the beam deflection scheme. When another source, such as an arc lamp and monochromator is used, the shape of the beam may not be well enough defined to permit adequate comparison with theory and the interferometer may be needed for quantitative comparisons. This would be more important in microscopic applications of the technique than in spectroscopic applications.

C. SURFACE QUALITY REQUIREMENTS

Criteria for the optical quality of the surface for photothermal displacement spectroscopy differ for the three detection schemes. For ATR, the surfaces of both the prism and the sample must be polished over a large area so that they can be brought to within 200 Å of each other in the region of interest. On the scale of the probe beam spot size, two regimes of the dimension of the surface roughness, Δ, need to be considered.

When the surface roughness is greater than the probe beam wavelength ($\Delta>\lambda$), but smaller than the probe beam spot size, the interferometer and ATR methods require the average variation over the wavefront, δ, to be much smaller than λ (e.g. apply the Rayleigh criterion: $\delta\leq\lambda/4$). For the beam deflection scheme, the average value of the slope (δ/Δ) must be smaller than the angular aperture of the detector (typically a few hundredths of a radian). This is readily achievable without polishing the sample.

When the dimension of the surface roughness is smaller than the probe beam wavelength ($\Delta<\lambda$), then the reflected wavefront is made of two components: a coherently reflected beam of uniform amplitude and well defined direction; and an incoherent beam with random amplitude and dispersed spatial distribution which generates a speckle pattern. The relative distribution of both components in space is a function of λ, the optical constants of the material being studied, and the surface roughness. Theoretical models exist[5] which enable the calculation of both components. Experimentally, we have found that the presence of a speckle of a few percent does not affect the sensitivity of the three detection schemes described in this paper.

IV. EXPERIMENTAL RESULTS AND COMPARISON WITH THEORY

Photothermal displacement data were obtained with all three of the above mentioned detection schemes. Experience showed the beam deflection (BD) method to be the simplest to use and to have the best long term stability of the three. Therefore, most of the results presented below were taken using the BD detection scheme. In general, the results carry over to the interferometric and ATR detection schemes. To characterize the technique, a number of experiments were conducted and the results compared with the predictions of equation 6. The dependence of the photothermal signal on incident power, relative position of the pump and probe beams, focussing, wavelength of the exciting beam, air pressure, and modulation frequency were studied using a silicon wafer, a copper slab, and assorted glass filters and thin films. These materials were chosen because of the large range in their thermal and optical properties. All experiments were performed at room temperature.

A. POWER DEPENDENCE

The power dependence of the signal is predicted by our theory to be linear over the range where the assumptions made in the computer calculation are valid (i.e. the linearized thermoelastic equations). Experimentally, this was found to be true over at least three orders of magnitude of incident power. It should be noted that changing the value of a surface absorption is equivalent to changing the incident power on a sample with a very large absorption coefficient, and thus linearity with the surface absorption coefficient is predicted. This has been verified experimentally using a thin amorphous silicon film.

B. RELATIVE BEAM POSITION

Using the beam deflection method, the signal maps out the slope of the photoinduced displacement as the pump beam is translated across the probe beam spot on the sample. Figure 2 depicts the magnitude (2a) and phase (2b) versus the relative position (r_0) of the two beams on didymium glass. The magnitude rises as the pump beam comes into the vicinity of the probe beam, then goes sharply to zero at the center of the overlap where the slope of the displacement at the probe beam position is zero. The signal then changes sign (phase shift by 180°) and repeats itself as a mirror image. Any deviation from mirror imaging is a strong function of the alignment of the beams (if the pump beam, probe beam and sample normal are all in the same plane), especially when light is absorbed throughout the sample. Inhomogeneities in the sample or the beam profile can also be detected.

The phase of the photothermal signal relative to the pump beam modulation also contains important information. As the pump beam is turned on, the heat is initially deposited where the beam intersects the sample. The heat then diffuses out from the center, and the peak signal occurs at a later time (a more negative phase) as the distance between pump and probe centers is increased (see Fig. 2b). For the glass sample, the thermal diffusivity ($=K_{th}/\rho C$) is such that the heat diffuses out in a few milliseconds. Beyond a few thermal lengths, mechanical coupling to the directly heated parts of the sample dominates, causing the phase to reach a constant value. The theoretical predictions for the magnitude and phase of the signal agree very well with the experimental findings, as shown in Fig. 2. The scaling of the height of the

experimental curve in Fig. 2a. was adjusted arbitrarily, but was found to be within the uncertainties of the pump beam power, position sensor sensitivity, and the thermal expansion coefficient of the glass. The shape of the phase vs. relative position curve changes with the relative values of the optical absorption length ($1/\alpha$), the sample thickness (L), the thermal diffusion length (L_{th}) and the pump beam radius on the sample (a). Further discussion of the information contained in the phase of the signal is given in Section V. By fitting the shape of the two curves, especially the phase vs. relative position (Fig. 2b), it was possible to determine the thermal diffusivity of the glass to be $4.2 \times 10^{-3} cm^2/sec$. This value is typical of silicate based glasses with metallic impurities[6] and is about half that of pure fused silica. A mismatch of ten percent in the thermal diffusivity can be easily distinguished in the quality of the curve fit.

C. SPECTROSCOPY AND VACUUM COMPATIBILITY

To test the spectroscopic feasibility of the technique and its vacuum compatibility, the pump beam wavelength was varied over an absorption band in didymium glass both at atmospheric pressure and in vacuum. The effect of saturation was investigated using an optical edge filter. The beam deflection result for didymium glass is shown as the solid line in Fig. 3. This spectrum was taken while the glass was mounted inside a vacuum chamber at atmospheric pressure (10^5 Pa). The dashed line in Fig. 3 is an identical spectrum with the chamber evacuated to a pressure of 2.7 Pa(20 mTorr). The signal does not depend on a coupling to the air adjoining the sample, as there was no significant change when the density of the air in contact with the sample was

changed by more than 10^4. This demonstrates that the measured effects are not due to any "mirage" type of effect[7] caused by heating of the air near the sample surface. Spectra taken with the interferometer (dotted line in Fig. 3) reproduce the beam deflection results, and also show no significant change with the pressure of the ambient gas. The dash-dotted line in Fig. 3 is the absorption coefficient of the sample, calculated from a transmission spectrum as

$$\alpha = (1/L)\log_e(I_{transmitted}/I_{incident}). \tag{15}$$

It is apparent from Fig. 3 that the photothermal displacement signal gives the same information as the conventional transmission measurement.

The theoretical prediction for the signal as a function of the optical absorption coefficient is shown in Fig. 4. It can be seen that the relevant thickness for saturation is the thermal length and not the sample thickness. The signal is linear over a large range of α, and can be approximated as linear over other ranges, although with a smaller slope, until $\alpha L_{th} \cong 1/2$. An additional increase in the signal after the expected saturation near $\alpha L_{th}=1$ is seen when the heating is non-uniform within the first thermal length from the sample surface. This is likely due to the bending of the sample in addition to the uniform expansion, increasing the height and slope of the displacement on the sample surface. In the case of an optically thin sample, and hence uniform heating, the signal varies with the thickness of the sample as

$$S \propto 1-\exp(-L/L_{th}) \tag{16}$$

Thus only the first few thermal lengths contribute to the signal. This can be useful in decreasing the role of a weak bulk absorption in mask-

ing a surface absorption.

The absorption spectrum of a 760 nm, ir-transmitting edge filter was measured to investigate saturation effects. The photothermal signal was found to continue to give spectroscopic information with increasing absorption long after the transmission measurement, which saturates as αL gets large, had ceased to yield any useful information. Comparison with the theoretical curve (Fig.4) enables the absorption coefficient to be extracted from the photothermal displacement data, even in the non-linear region. The magnitudes of the measured and calculated signals were found to agree within the uncertainty of the material parameters of the glass.

D. FREQUENCY DEPENDENCE

The dependence of the photothermal displacement signal on the modulation frequency of the pump beam is different for bulk and surface absorptions, as discussed in Section V-B. It also varies with the relative size of the pump beam radius and the thermal length. If the pump beam radius is much larger than the thermal length at a given frequency, then the signal decays approximately as 1/f with a further increase in frequency. At lower frequencies where the pump beam is comparable to or smaller than the thermal length, the decay is slower. Experimentally, the beam deflection signal for a weakly absorbing, low thermal conductivity, glass sample illuminated with a beam focussed to a radius of 300 microns decayed as 1/f for frequencies greater than 6 Hz (L_{th} < 150 microns). At the other extreme, the BD signal at 2000 Hz ($L_{th} \cong 140\mu$) for a strongly absorbing, high thermal conductivity, copper sample illuminated with a beam of radius 75 microns was still over half the low

frequency value. For a given sample with both surface and bulk absorptions, the surface signal decays more slowly and can thus be differentiated from the bulk. This also has been verified experimentally [8].

V. DISCUSSION

A. GENERAL COMMENTS

Photothermal displacement can be used in many hostile environments as a non-perturbative probe due to the absence of the physical coupling found in other photothermal spectroscopies. For example, the optical properties and degree of homogeneity of a thin film can be monitored *in situ* during film deposition, or the deformation and absorption of laser mirrors can be monitored during pulsed operation. Experimentally, we have detected inhomogeneities and discontinuities such as pinholes in a thin film, as well as local variations in the thickness of the film itself.

The direct measurement of absorbed energy by photothermal displacement spectroscopy means the signal is proportional to the product of the incident power and the absorption coefficient, so the signal from optically thin materials can be enhanced by increasing the incident power. As mentioned in Section III, absorptions of 10^{-6}/Watt can be seen easily on a glass sample. This is not the case in traditional reflection and transmission experiments, however, where one is limited by the ability to measure absolute intensities. In a differential reflectivity measurement, the absolute value of $\Delta R/R$ can be determined to about 1%, and differential measurements of $\Delta R/R$ of a few times 10^{-4} can be measured[9], limiting sensitivity to 10^{-4} independent of the pump beam power.

Photothermal displacement should prove quite useful in the performance of optical spectroscopy of surface electronic states and adsorbates. Such investigations, which require ultrahigh vacuum and a wide

range of temperatures, have been difficult to pursue with traditional techniques. Optical absorption due to surface states will be easiest to investigate with photothermal displacement spectroscopy when there is minimal background from the substrate absorption, such as semiconductors in the energy gap or metals in the infrared. In this case small changes in the surface absorption will appear against little or no background. However, even if all of the unreflected probe beam is absorbed by the substrate in the first thermal length, a change in the reflectivity due to surface states will cause an equal and opposite change in the amount of energy absorbed, and hence detected. If the reflectivity is greater than 50%, the surface absorption will cause a greater relative change in the photothermal signal than in the reflected intensity.

B. SURFACE VS. BULK INFORMATION

Photothermal displacement spectroscopy is not only sensitive both to surface and bulk absorption of light, but can also distinguish between the two. This differs from traditional reflection and transmission spectroscopies for which the sample or optical alignment must be modified to determine where in the sample the absorption is occurring. This difference can be seen clearly in both the magnitude and the phase of the signal. Calculated curves for the BD signal from a silicon sample are shown in Fig. 5 for surface (5b and 5d) and bulk (5a and 5c) absorptions at three different modulation frequencies.

The behavior of the magnitude vs. position curves (5a and b) is quite different for the cases of uniform and surface heating of a thermally thick sample both in the lineshape at any one frequency and in the variation of the lineshape as the frequency (and hence thermal length)

is changed. When the sample is heated uniformly over the length of the sample ($\alpha L \ll 1$), the heat flow is radial and there is a contribution to the signal from the same heated thickness at all radii. The signal decays approximately exponentially with beam separation once outside the centrally heated region (see especially the 20 Hz. curve). When the thermal length becomes comparable to the pump beam radius it becomes difficult to separate the exponential and Gaussian components of the slope, but the signal extends further than would be expected for a pure Gaussian displacement with no heat flow. When the thermal length is much larger than the pump beam waist, as is the case in the 20 and 320 Hz curves in Fig. 5a, the area heated by the beam is proportional to the square of the thermal length, and hence is inversely proportional to the modulation frequency. This dependence would cancel the 1/f behavior of the signal due to the time the pump beam has to deposit energy each cycle (see Eq. 2) if there were no other dependence on the frequency. The slow decay of the signal magnitude with increasing frequency in Fig. 5a is due to less of the heated sample contributing to the effective length of expansion as the thermal length decreases. The decay of the slope with frequency is slower than that of the displacement itself for both surface and bulk absorption due to the extra weighting the Gaussian gives the slope. The implications of this to imaging and microscopy are discussed in Section V-D. When the sample is thermally thin, the bulk absorption signal decays more slowly than in the thermally thick case, as would be expected with no possible change in the effective length of expansion.

When the sample is heated only at the surface and the thermal length is larger than the pump beam radius, the heat flow is hemispherical, and a larger effective length contributes to the signal at the center of the displacement than further out. This feature makes the surface signal decay much more quickly with relative beam position than the bulk signal outside the central region. There is also no interior heated region to be accessed by a larger thermal length as in the uniformly heated case, hence the peak signal changes little as the thermal length varies from 16a to 4a. As the thermal length becomes smaller, however, the heated area is more heavily weighted by the constant pump beam radius and the signal starts to decay, eventually approaching the 1/f dependence referred to in (2). This is true for both surface and bulk absorptions.

The behavior of the phase of the signal relative to the pump beam modulation is also quite different for surface and bulk absorptions. In the limit where $a > \sim 2L_{th}$, there is little heat flow in the radial direction beyond the initially heated region. Thus in this limit the primary contribution to the slope at the surface is from mechanical coupling to the region $r<a$. If there is uniform heating over the first few thermal lengths of a thermally thick sample, then the phase rapidly approaches a value near -90°. This value is the one expected if there were no heat flow, with the expansion being the time integral ($\sin(\omega t)$) of the optical heating ($\cos(\omega t)$). If the heat is deposited at the surface of the sample, then the phase approaches a value near -45°. The difference in timing occurs because in the surface heating case the heat diffuses to the rear of the sample, whereas in the uniform heating case the column

of material heated by the pump beam is heated simultaneously.

When the pump beam 1/e radius is smaller than $\sim 2L_{th}$, there is more structure in the phase. On a thermally thin sample ($L < \sim L_{th}$), uniform optical heating induces a slope whose phase varies linearly with relative beam position as one goes out from the center. The rate is near one radian/L_{th}, the value expected for uniform thermal diffusion where the only heat flow is radial (see dashed line in Fig. 5c). Surface heating on the same sample, however, causes the heat to diffuse into the sample as well as radially, and the behavior of the phase is quite different. Initially, the phase shows the peak signal occurring at a later time as one probes further out from the center, as occurs in the optically thin case outlined above, but when the relative beam position is such that the mechanical coupling to the rear of the sample which is expanding as heat diffuses directly into the sample, is stronger than the expansion due to radial heat diffusion, the phase approaches an asymptotic value near -45° (see dashed line in Fig 5d).

On a thermally thick sample, it is the optically thick sample (surface heating) which causes the phase of the peak signal to vary linearly with relative beam position over a large region. The rate of heat flow in this case, however, is about twice that of the sample which is optically and thermally thin, or about $27^{o}/L_{th}$. The phase of the signal does eventually approach -45°, but it does so much later than in the thermally thin case (see, e.g., the two curves at 320 Hz. in Fig. 5d). When a thermally thick sample is uniformly heated, the phase tends toward an asymptotic value near -90° (see Fig. 5c) after a few thermal lengths. The mechanical coupling to the back of the sample is again

dominating out from the center of the displacement.

The asymptotic phase regime occurs in an experimentally accessible region (i.e. when there is still significant signal to determine the phase accurately) when $a > \sim L_{th}/4$ and occurs closer to the center as L_{th} decreases. When the sample is uniformly heated, the constant phase region occurs closer to the center as L increases; with surface heating it occurs further out as L increases (see Figs. 5c and 5d). The value of the asymptotic phase varies with α and L. The transition region for a thermally thick sample between large α ($\phi_{as} \sim -40$ to -45 degrees) and small α ($\phi_{as} \sim -85$ to -95 degrees) occurs near $\alpha L_{th} = 1$. Changing L, the sample thickness, shifts ϕ_{as} within the ranges indicated.

C. DEDUCING THERMAL INFORMATION

Thermal properties of a sample can be obtained most accurately from the slope of the photothermal displacement by fitting the magnitude and phase versus position curves to Eq. 6; the needed input information is the radius of the pump beam, the absorption coefficient, the sample thickness and the modulation frequency. Curve fitting is necessary when the phase reaches an asymptotic value before a linear range is established or with semitransparent samples. The cases of thermally thin samples ($L < \sim 2L_{th}$) with uniform heating ($\alpha L \ll 1$) and thermally thick samples with surface heating yield linear changes of phase with position beyond a central flat region which is approximately equal to the directly heated area. In the first case (optically and thermally thin), the phase shifts approximately $53^{\circ}/L_{th}$ and in the second case (optically and thermally thick), the phase shifts approximately $27^{\circ}/L_{th}$. The latter is also the case for thermally thin opaque materials before the

asymptotic regime of the phase. As long as the pump beam radius (a) is less than L_{th}, the phase beyond a few a is dominated by thermal diffusion and is essentially independent of a. The magnitude of the signal, however, is sensitive to a, both in size and shape. Experimentally, the variation of phase with relative beam position on a copper block (thermally thick) and a silicon wafer (thermally thin) was found to agree quite well with this simple formula of $27^{o}/L_{th}$ when the condition of $a<L_{th}/4$ was met. When a 4 micron thick, absorbing film of amorphous silicon on a transparent sapphire substrate was investigated, the phase changed at a rate of $27^{o}/L_{th}$ of the sapphire, indicative of surface absorption on the substrate.

D. IMPLICATIONS FOR MICROSCOPY AND IMAGING

Optical and thermal imaging and microscopy can be readily performed using photothermal displacement detection. In addition, subsurface structures can be detected in a nondestructive manner by varying the modulation frequency of the pump beam. The interferometer has already been proposed in this mode[10]. However, the beam deflection scheme should be easier to implement because of the less stringent demands on the sample alignment as the sample and beam are moved relative to each other. In other photothermal techniques, the information obtained is averaged over the thermal diffusion length both vertically into the sample and radially out from the optical excitation, and thus focussing the pump beam more tightly than the thermal diffusion length causes little change in the signal. However, the radial derivative of the surface displacement, as detected in the beam deflection scheme, gives more localized optical information than the magnitude of the displacement, as

detected by the interferometer or ATR, or than other more traditional photothermal techniques. In the beam deflection scheme, the signal continues to increase as the pump beam is focussed more tightly than the thermal diffusion length. This is because the maximum slope has an additional inverse dependence on a in the Gaussian, directly heated region, but the slope does not change significantly with a in the exponentially decaying diffusively heated region. The position of maximum slope moves out slowly from the $a/\sqrt{2}$ of a pure Gaussian shaped displacement as the thermal length is increases, but even when the thermal length is fifteen times the radius of the pump beam, the point of maximum slope is less than three times the pump radius (see Fig. 5). The steepest part of the displacement, and hence the point of maximum slope, is governed primarily by the Gaussian shaped, directly heated area and thus the information obtained is heavily weighted by this region.

When the pump beam is more tightly focussed than the probe beam, and both radii are smaller than the thermal length, the signal magnitude acts as though the effective pump beam radius is $(a^2 + b^2)^{1/2}$, where a and b are the 1/e radii of the pump and probe beams, respectively. A simple argument for this behavior can be seen in the limit of no thermal diffusion, where the displacement is Gaussian. The position sensor integrates the deflection of the entire probe beam, weighted by the probe beam intensity. This yields a signal of the form

$$S = 2hr_0/(a^2+b^2)\exp(-r_0^2/(a^2+b^2)) \tag{17}$$

Thus with a Gaussian probe, the signal can be expressed in the same form

as the slope with a, the pump radius, replaced by the pythagorean sum of the pump and probe radii. The prefactor h, however, should be a function of a and not $(a^2+b^2)^{1/2}$ since it includes the heated area. If the thermal length is dominating the size of the heated area, however, then the substitution of the pythagorean sum of the two radii for a is valid and should agree with the experimental data. This was found to be the case. The radial resolution for microscopy is thus dependent on the size of both the pump and probe beams.

VI. CONCLUSION

We have presented three different forms of photothermal displacement spectroscopy: beam deflection, interferometry and attenuated total reflection. The beam deflection method was found to be the easiest of the three to implement, and should therefore prove to be the most useful. The technique is simple and readily applicable to use in ultrahigh vacuum. It is possible to distinguish surface absorptions from those occurring uniformly throughout the first thermal length of the sample, and a wide variety of materials can be investigated with minimal sample preparation. Therefore, photothermal displacement spectroscopy should prove a very useful tool for the study of the optical properties of surfaces and thin films.

The experimental results were shown to be well predicted by a linearized thermoelastic theory, as contained in the Navier-Stokes equation. The photothermal signal is linear in the pump beam power, independent of the (gaseous) ambient medium, and linear in the absorption coefficient over a large range. The thermal diffusivity of the material can be extracted easily from the shape of the signal vs. relative beam position curves. The technique should be applicable over a wide temperature range since the absolute temperature enters into the signal only indirectly, as the thermal expansion coefficient and thermal diffusivity vary with temperature. In addition, photothermal displacement detection should prove to be a useful tool for performing microscopy, imaging, and nondestructive depth profiling of materials.

Acknowledgements: This work was supported by the Office of Energy Research, Physical and Technological Research Division of the U. S.

Department of Energy Contract No. DE-AC03-76 SF00098; and by DARPA Contract No. 3343.

APPENDIX

The surface displacement was calculated for an infinite slab of thickness L (extending infinitely in the radial direction and from 0 to L in the z direction), assuming no normal stress or heat conduction at the boundaries z=0 and z=L. The solution to the Navier-Stokes equation

$$(1-2\nu)\ \nabla^2 u + \nabla(\nabla\cdot u) = 2(1+\nu)\alpha_{th}\ \nabla T \tag{A1}$$

where u = displacement vector
ν = Poisson ratio
T = change in temperature from equilibrium value
and α_{th} = thermal expansion coefficient,

is the sum of a particular solution $u_p = \nabla\Phi$ where

$$\nabla^2\Phi = \alpha_{th}T(1+\nu)/(1-\nu) \tag{A2}$$

and a solution to the homogeneous equation, which for this cylindrical symmetry is given by

$$u_h = (1/(1-2\nu)[(\partial^2\phi\ /\partial r\partial z)\hat{r} + (2(1-\nu)\ \nabla^2\phi - (\partial^2\phi\ /\partial z^2)\hat{z}] \tag{A3}$$

where ϕ is the Love function [11] satisfying $\nabla^2\nabla^2\phi = 0$. The normal stress components, σ_{rz} and σ_{zz}, are given by

$$\begin{aligned}
\sigma_{rz_p} &= 2\mu(\partial^2\Phi/\partial r\partial z) \\
\sigma_{rz_h} &= (2\mu/(1-2\nu))\partial/\partial r[(1-\nu)\nabla^2\phi - \partial^2\phi/\partial z^2] \\
\sigma_{zz_p} &= 2\mu(\partial^2\Phi/\partial z^2 - \nabla^2\Phi) \\
\sigma_{zz_h} &= (2\mu/(1-2\nu))\ \ \partial/\partial z\ [(2-\nu)\nabla^2\phi - \partial^2\phi/\partial z^2]
\end{aligned} \tag{A4}$$

where μ = shear modulus

At the boundaries, z=0 and z=L, σ_{rz} and σ_{zz} must be zero. For this

geometry, the solution to A2 can be expressed as the integral of a Green function over the temperature, as [12]

$$\Phi(r,z) = -\alpha_{th}(1+\nu)/(1-\nu)\int_0^\infty dk\int_0^\infty \rho\, d\rho\int_0^L d\zeta\, \{T(\rho,\zeta)J_0(kr)J_0(k\rho) \times [\sinh(kz_<\sinh(k(L-z_>))/\sinh(kL)]\} \tag{A5}$$

where $z_<$ = the minimum of z and ζ and $z_>$ = the maximum of z and ζ. The solution for the temperature profile in the limit of no heat flow at the boundaries is[4b]:

$$T(r,z,t) = (1/2)\int_0^\infty \Delta d\Delta\, N(\Delta)M(\Delta,z)J_0(\Delta r/z)\exp(i\omega t) \quad + c.c. \tag{A6}$$

where

$$N(\Delta) = -(\alpha P/4\pi K_{th})\exp(-\Delta^2 a^2/4L^2)/[(\alpha L)^2 - S^2]$$

$$M(\Delta,z) = \exp(-\alpha z) + C_1\exp(-Sz/L) - C_2\exp(Sz/L)$$

$$C_{1,2} = (\alpha L/S)[\exp(-\alpha L) - \exp(\pm S)]/[2\sinh(S)]$$

$$S^2 = \Delta^2 + i(\omega\rho C/K_{th})L^2$$

$$= \Delta^2 + i(L^2/2L_{th}^2)$$

K_{th} = thermal conductivity
ρ = mass density
C = heat capacity/gram

The first term in M represents the direct heat input from the optical absorption and the final two terms are the forward and reverse thermal waves. Solving for the particular solutions for the displacement normal to the surface and the normal stresses, one finds

$$u_{z_p}(r,0) = -\alpha_{th}(1+\nu)/(1-\nu)\int_0^\infty kdk\int_0^\infty \rho\, d\rho\int_0^L d\zeta\{T(\rho,\zeta)J_0(kr)J_0(k\rho) \times \sinh(kL-k\zeta)/\sinh(kL)\}$$

$$\sigma_{rz_p}(r,0) = 2\mu\alpha_{th}(1+\nu)/(1-\nu)\int_0^\infty k^2dk\int_0^\infty \rho\, d\rho\int_0^L d\zeta\{T(\rho,\zeta)J_0(kr)J_0(k\rho) \times \sinh(k\zeta)/\sinh(kL)\}. \tag{A7}$$

$$\sigma_{rz_p}(r,L) = -2\mu\alpha_{th}(1+\nu)/(1-\nu)\int_0^\infty k^2 dk \int_0^\infty \rho\, d\rho \int_0^L d\zeta\{T(\rho,\zeta)J_0(kr)J_0(k\rho) \times \sinh(kL - k\zeta)/\sinh(kL)\}.$$

$$\sigma_{zz_p}(r,z=0,L) = 0.$$

The general solution to $\nabla^2\nabla^2\phi(r,z)=0$ has the form:

$$\phi(r,z)=\int_0^\infty dk J_0(kr)\{[A+B(kz-\Delta/2)]\sinh(kz-\Delta/2) + [C+D(kz-\Delta/2)]\cosh(kz-\Delta/2)\} \tag{A8}$$

where $\Delta = kL,$

and then

$$\begin{aligned} u_{z_h}(r,0) &= 1/(1-2\nu)\int_0^\infty k^2 dk J_0(kr)\{\sinh(\Delta/2)[A-B\Delta/2-2D(1-2\nu)] \\ &\quad + \cosh(\Delta/2)[-C+D\Delta/2 + 2B(1-2\nu)]\} \\ \sigma_{rz_h}(r,z=0,L) &= 2\mu/(1-2\nu)\int_0^\infty k^3 dk J_1(kr)[\mp\sinh(\Delta/2)(A \mp B\Delta/2+2D\nu) \\ &\quad + \cosh(\Delta/2)(C \mp D\Delta/2+2B\nu)] \\ \sigma_{zz_h}(r,z=0,L) &= 2\mu/(1-2\nu)\int_0^\infty k^3 dk J_0(kr)\{\mp\sinh(\Delta/2)(-C \pm D\Delta/2+B(1-2\nu)] \\ &\quad + \cosh(\Delta/2)[-A \pm B\Delta/2+D(1-2\nu)]\} \end{aligned} \tag{A9}$$

Solving for the four unknowns, A, B, C, and D, subject to the four boundary conditions

$$\begin{aligned} \sigma_{rz}(r,0) &= 0 \qquad & \sigma_{rz}(r,L) &= 0 \\ \sigma_{zz}(r,0) &= 0 \qquad & \sigma_{zz}(r,L) &= 0 \end{aligned} \tag{A10}$$

one finds

$$\begin{aligned} A &= I_1[(1-2\nu)\cosh(\Delta/2) - \Delta/2\sinh(\Delta/2)]/[\sinh(\Delta) + \Delta] \\ B &= I_2\sinh(\Delta/2)/[\sinh(\Delta) - \Delta] \\ C &= I_1[(1-2\nu)\sinh(\Delta/2) - \Delta/2\cosh(\Delta/2)]/[\sinh(\Delta) - \Delta] \\ D &= I_2\cosh(\Delta/2)/[\sinh(\Delta) + \Delta] \end{aligned} \tag{A11}$$

where $I_1 = 2\alpha_{th}(1-2\nu)(1+\nu)/(1-\nu)\int_0^\infty \rho d\rho \int_0^L d\zeta J_0(k\rho)\{T(\rho,\zeta)\sinh(\Delta/2)$
$\times \cosh(k\zeta - \Delta/2)/k \sinh(\Delta)\}$

and $I_2 = 2\alpha_{th}(1-2\nu)(1+\nu)/(1-\nu)\int_0^\infty \rho\, d\rho \int_0^L d\zeta J_0(k\rho)\{T(\rho,\zeta)\cosh(\Delta/2)$
$\times \sinh(k\zeta - \Delta/2)/k \sinh(\Delta)\}$.

Note that A and D [B and C] are non-zero for a temperature distribution which is even [odd] across the slab. The use of two Green functions, one for temperature and the other for the displacement, has the unfortunate consequence that u_z (r,0) is not integrable in this form. However, $(\partial u_z/\partial r)(r,0)$ is finite and integrable. For the simplest detection scheme described here, beam deflection, the measured quantity is $(\partial u_z/\partial r)(r,0)$, hence it was calculated. The height of the displacement can then be calculated by integrating the slope over r. The net result for the slope is:

$$\frac{\partial u_z}{\partial r}(r,o) = -\frac{\alpha_{th}\,\alpha P(1+\nu)}{16\pi K_{th}(1-\nu)}\left[\int_0^\infty \frac{\Delta^2 d\Delta J_1(\Delta r/L)\exp(-\Delta^2 a^2/4L^2)}{\sinh\Delta[(\alpha L)^2 - S^2]} \times \right.$$

$$\{[A_o(-\alpha L)+B_1A_1(-\alpha L)+B_2A_2(-\alpha L)]+C_1[A_o(-S)+B_1A_1(-S)+B_2A_2(-S)]$$

$$\left. +C_2[A_o(S)+B_1A_1(S)+B_2A_2(S)]\}+C.C.\right] \qquad \text{(A12)}$$

where
$$A_0(x) = (2/L)\int_0^L d\zeta \exp(x\zeta/L)\sinh(\Delta - \Delta\zeta/L)$$
$$A_1(x) = (2/L)\int_0^L d\zeta \exp(x\zeta/L)\cosh(\Delta\zeta/L - \Delta/2)$$
$$A_2(x) = (2/L)\int_0^L d\zeta \exp(x\zeta/L)\sinh(\Delta\zeta/L - \Delta/2)$$
$$B_1(\Delta) = -\sinh(\Delta/2)[\Delta - (1 - 2\nu)\sinh(\Delta)]/[\Delta + \sinh(\Delta)]$$
$$B_2(\Delta) = \cosh(\Delta/2)[\Delta + (1 - 2\nu)\sinh(\Delta)]/[\Delta - \sinh(\Delta)]$$

and C_1 and C_2 are defined after equation A6. This equation is the same

as equation 6 in the main text when the integrals for the A(x) terms are calculated. The three sets of terms in square brackets are from the three exponential terms in the temperature distribution-- the optical absorption decay and the forward and reverse thermal waves. The three terms within the square brackets are from the particular solution to the Navier-Stokes equation (u_p) and the symmetric and antisymmetric parts to the homogeneous solution (u_h).

In calculating the signal, the parameters for crystalline silicon and fused silica were taken from Sze[13] and the AIP Handbook[14].

REFERENCES

[1] H. Lüth, Appl. Phys., 8, 1, (1975).

[2] G. Heiland and W. Mönch, Surf. Sci., 37, 30, (1973).

[3] A. Hordvick, Appl. Opt., 16, 2827, (1977).

[4] Other photothermal techniques include photoacoustic spectroscopy (see, for example, Optoacoustic Spectroscopy and Detection, Y.-H. Pao, Ed., (Academic Press, New York, 1977); W. B. Jackson and N. M. Amer, J. Appl. Phys., 51, 3343, (1980)), and photothermal deflection spectroscopy (W. B. Jackson, N.M. Amer, A.C. Boccara, and D. Fournier, Appl. Opt., 20, 1333, (1981)). However, those techniques are not suited for experiments which require ultrahigh vacuum, cryogenics or the high temperatures necessary for annealing many materials.

[5] See, for example, I. Uhlidal, F. Lubes, and K. Navratil, J. Phys. (Paris), 11, C5-77, (1977).

[6] Y. S. Touloukian, R. W. Powell, C. Y. Ho, M. C. Nicolaou, "Thermal Diffusivity", Thermophysical Properties of Matter, Vol. X, (IFI/Plenum, New York, 1973)

[7] A. C. Boccara, D. Fournier, and J Badoz, Appl. Phys. Lett., 36, 130, (1980); and A. C. Boccara, D. Fournier, W. Jackson, and N. M. Amer, Opt. Lett., 5, 377, (1980).

[8] M. A. Olmstead and N. M. Amer, submitted to J. Vac. Sci. Technol.

[9] E. D. Huber & S. O. Sari, Rev. Sci. Instrum., 50, 438, (1979).

[10] S. Amer , E. A. Ash, V. Neumann, C. R. Petts, Electron. Lett., 17, 337, (1981).

[11] W. Nowacki, Thermoelasticity, (Pergammon, Oxford,1962).

[12] J. D. Jackson, Classical Electrodynamics, (John Wiley & Sons, New York, 1975), p. 132.

[13] S. M. Sze, Physics of Semiconductor Devices, (John Wiley & Sons, New York, 1981).

[14] American Institute of Physics Handbook, D. E. Gray, Ed., (McGraw-Hill, New York, 1972).

FIGURE CAPTIONS

Figure 1. Experimental configuration for a) beam deflection, c) interferometric and d) attenuated total reflection detection schemes. b) An expanded view of the displacement for the beam deflection configuration. The reflected probe beam alternates between paths a and b as the surface is displaced.

Figure 2. Beam deflection(BD) signal vs. the relative position (r_0) of the pump and probe beams. The circles are experimental points of the a) amplitude and b) phase of the BD signal as the pump beam is translated across the sample (see inset). The sample is 0.25 cm thick didymium glass with an absorption coefficient at the wavelength used of 5.4 cm^{-1}. The pump beam 1/e radius was 100 microns at the sample and the modulation frequency was 13.8 Hz. The solid lines are the slope magnitude and phase calculated from equation 6 using a thermal diffusivity of 4.2×10^{-3} cm^2/sec and the above experimental parameters. A ten percent variation in the thermal diffusivity is readily detectable in the quality of the curve fit. The units of the theoretical curve are for an incident power of one milliwatt and a thermal expansion coefficient of $5.1 \times 10^{-6} K^{-1}$.

Figure 3. Photothermal signal vs. wavelength. An absorption spectrum of 0.25 cm thick didymium glass obtained by photothermal displacement spectroscopy. The modulation frequency was 17 Hz (interferometer at 14 Hz); the thermal length is thus about 100 microns. The solid line is the beam deflection signal at atmospheric pressure, the dashed line is the BD signal at a pressure of 20 mTorr, the dash-dotted line is the absorption coefficient as calculated from a transmission measurement and

the dotted line is the same spectrum taken by the interferometer method at atmospheric pressure. The power of the pump laser (Kr^+ pumped oxyzene dye laser) was about 7 mW at the lower edge of the spectrum and 60 mW at the center.

Figure 4. Theoretical slope vs. optical absorption coefficient. Results from equation 6 of the photoinduced slope 100 microns from the pump beam center as the absorption coefficient is varied from 0 to 5 cm^{-1} and from 0 to 500 cm^{-1}. Note the different scales for the two curves. The slope is calculated for a sample of length 0.25 cm, thermal expansion coefficient of $5x10^{-7}K^{-1}$, thermal diffusivity of $8.2x10^{-3}$ cm^2/sec and a Poisson ratio of 0.25. These parameters are typical of fused silica. The modulation frequency is 14.2 Hz giving a thermal length of 135 microns. The pump beam was assumed to be one milliwatt of incident power focussed to a beam radius of a=100 microns. The linear dependence of the signal on the absorption coefficient at low absorption and the saturation when $\alpha L_{th}>>1$ are clearly seen.

Figure 5. Theoretical signal vs. relative beam position for different absorption and thermal lengths. Results of equation 6 for a silicon sample .33 cm (.033 cm) thick are shown as the solid (dashed) curves. The amplitude (5a and 5b) and phase (5c and 5d) are shown for a weak bulk absorption (5a and 5c) and a surface absorption (5b and 5d) for frequencies of 20, 320 and 5120 Hz. The thermal lengths for these frequencies are 1200, 300 and 75 microns, respectively, using a thermal diffusivity of 0.90 cm^2/sec. The pump beam was assumed to be a one milliwatt beam focussed to a 1/e radius of 75 microns, and the thermal expansion coefficient was taken to be $2.6x10^{-6}$ K^{-1}.

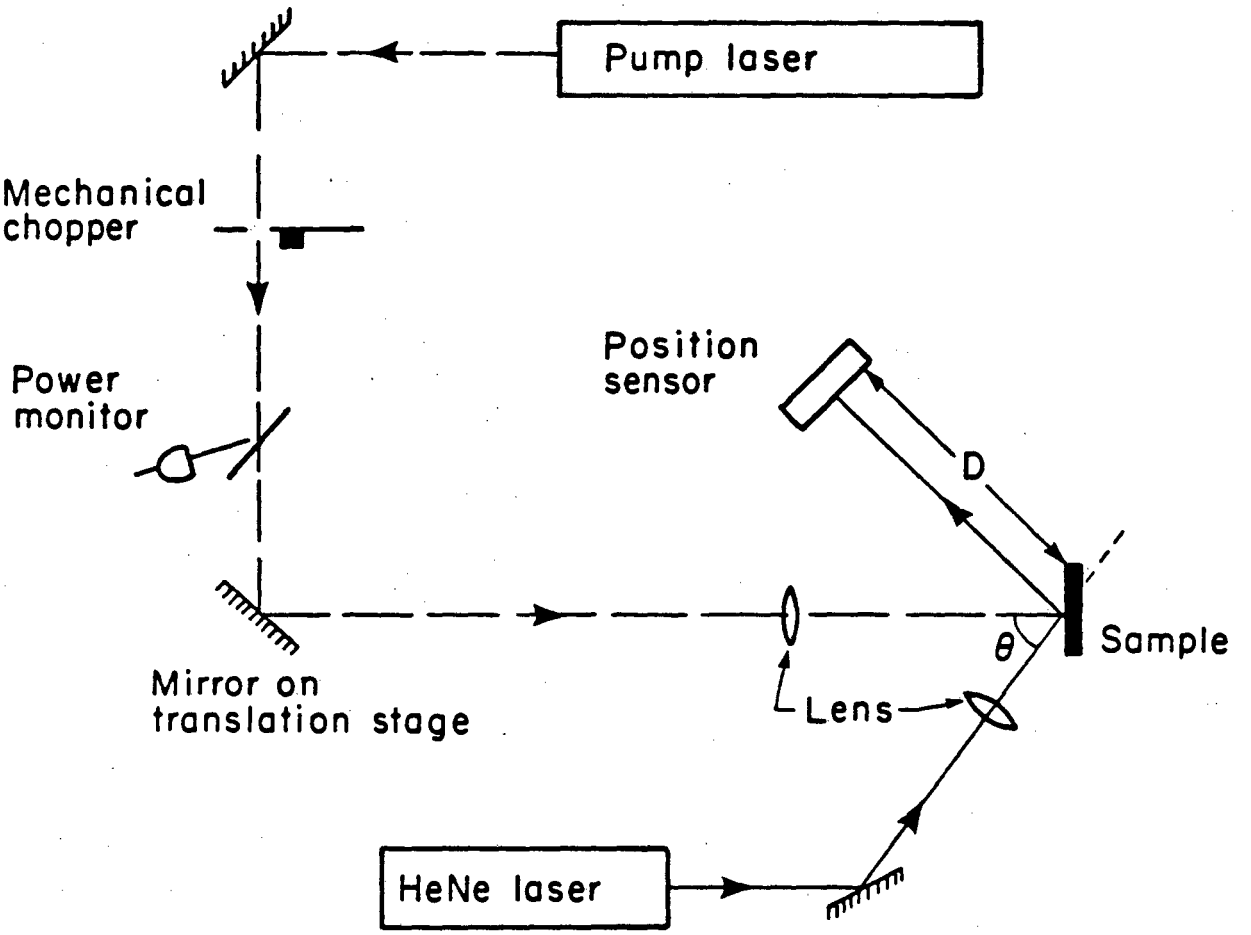

XBL 831 - 22

Figure 1a

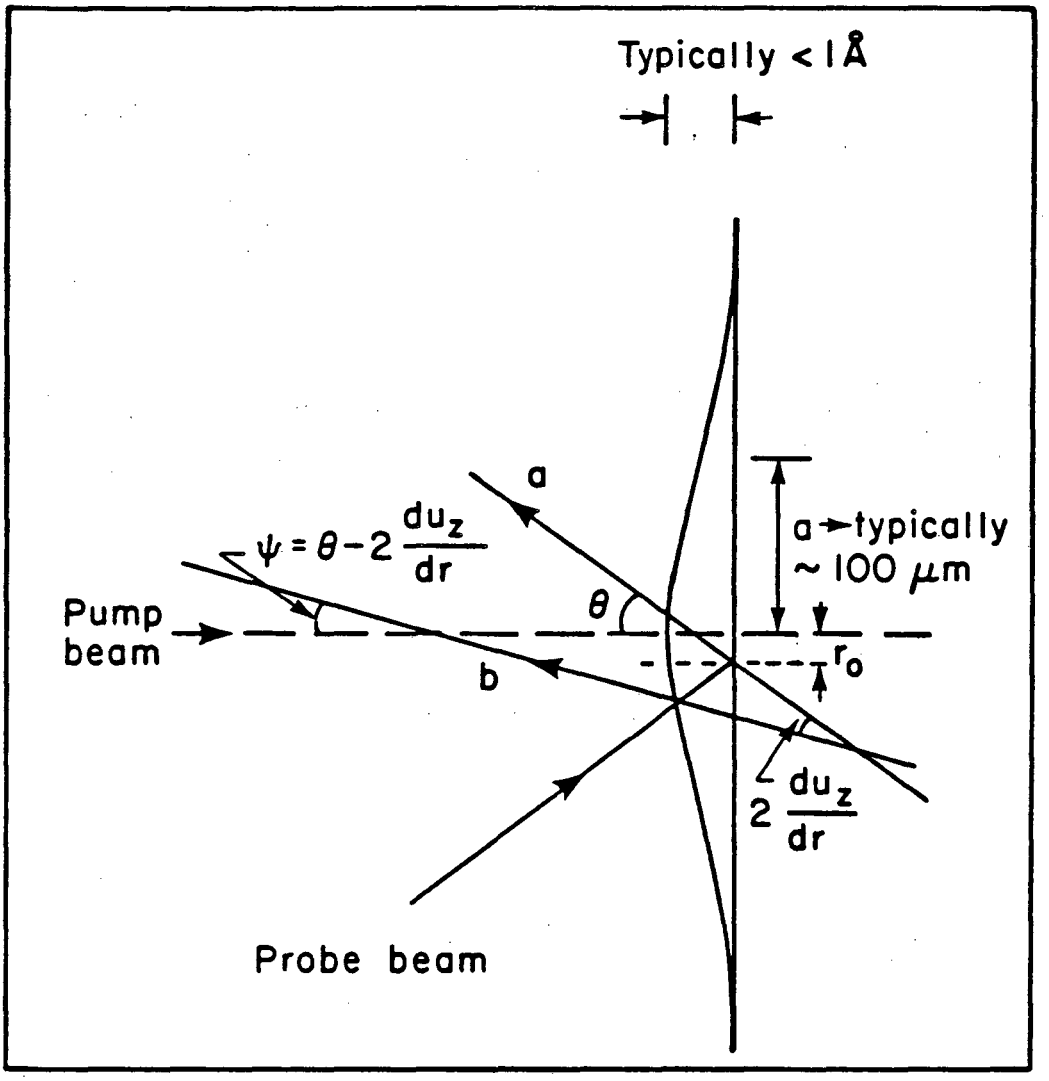

XBL 832-7778

Figure 1b

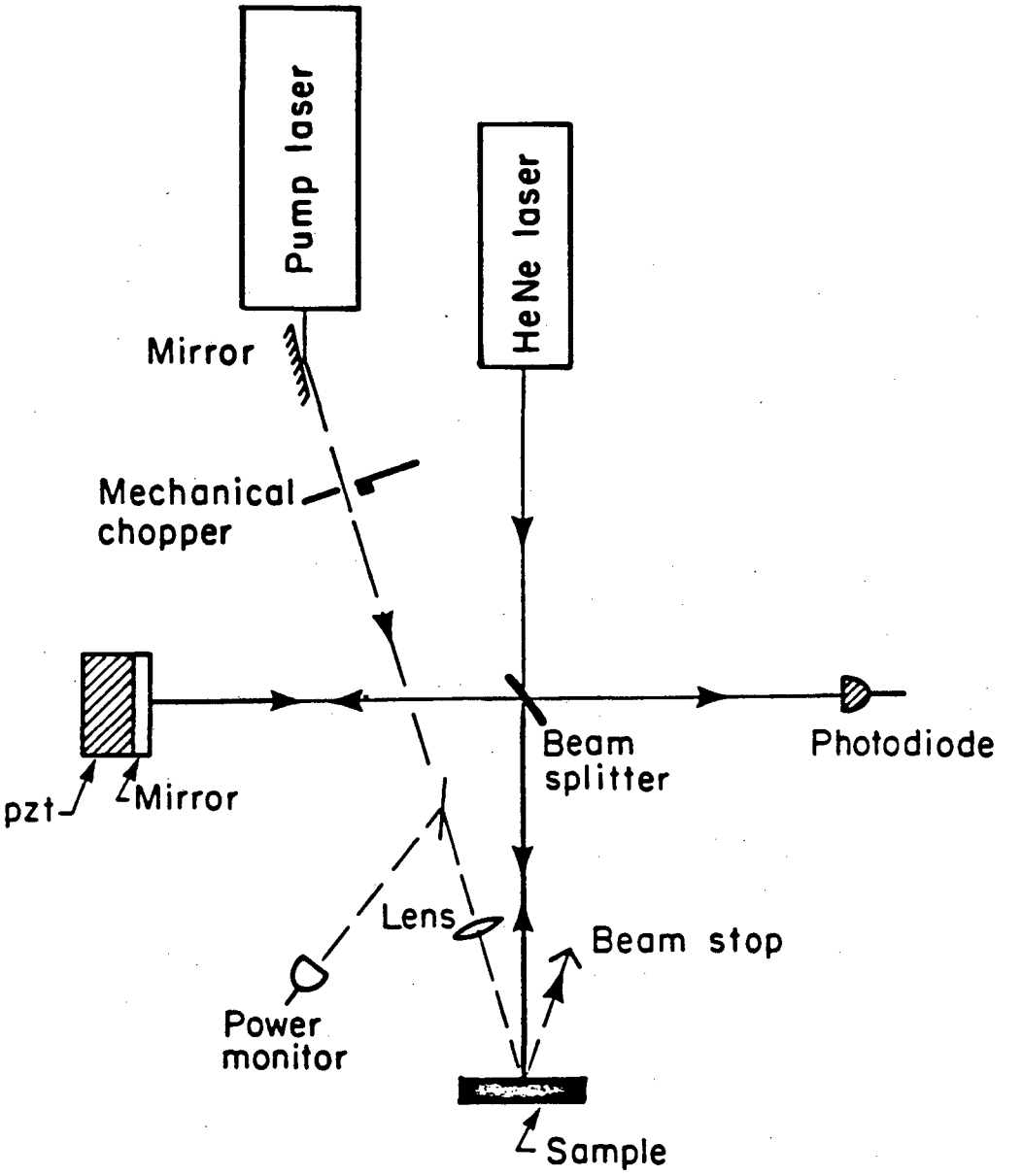

XBL 832-7779

Figure 1c

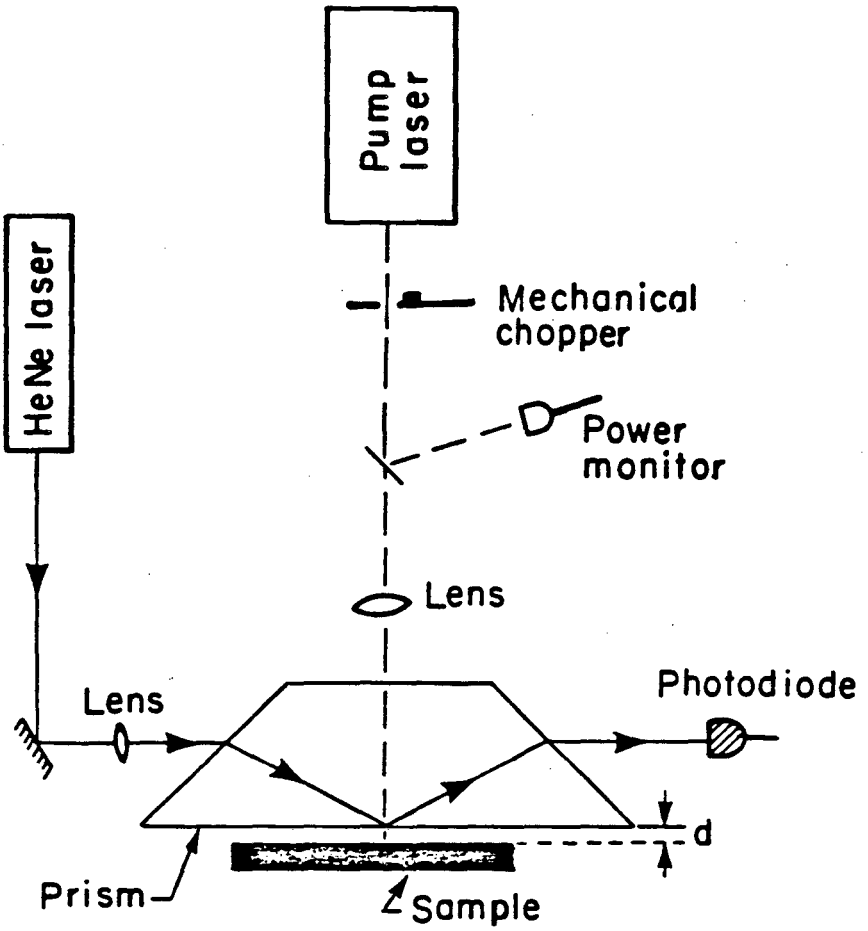

XBL 831 - 21

Figure 1d

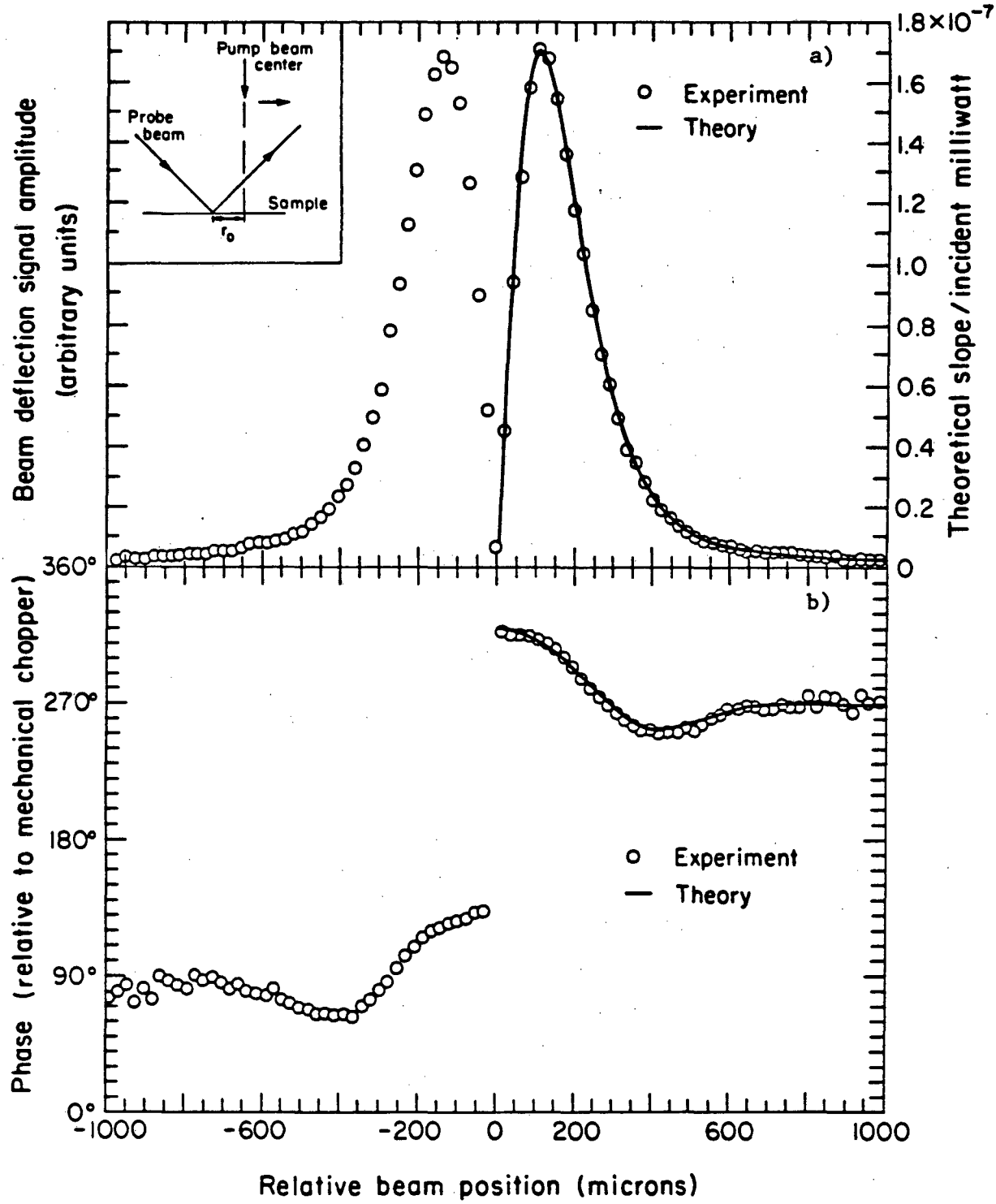

XBL 831 - 19

Figure 2

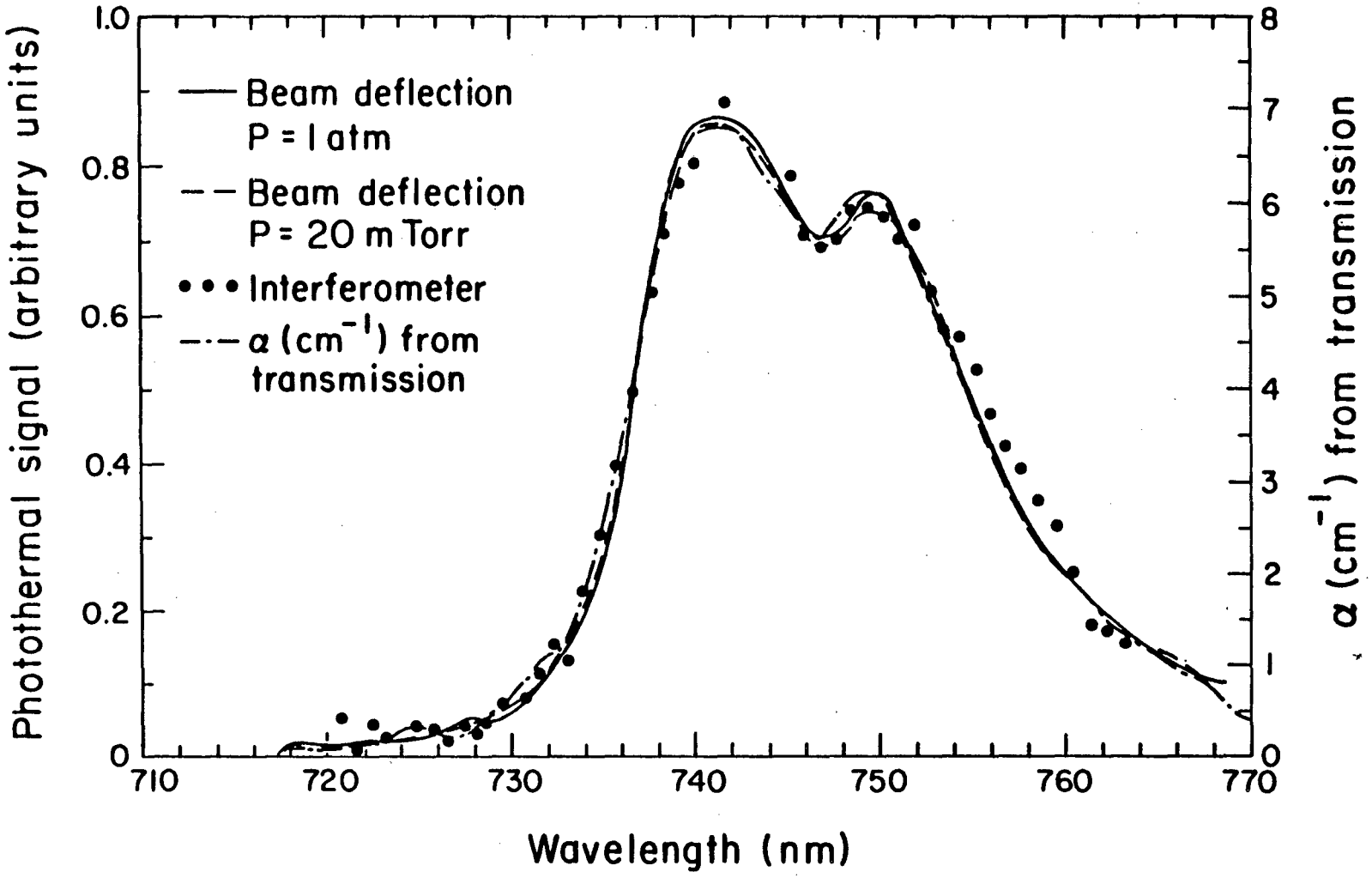

Figure 3

XBL 831 - 20

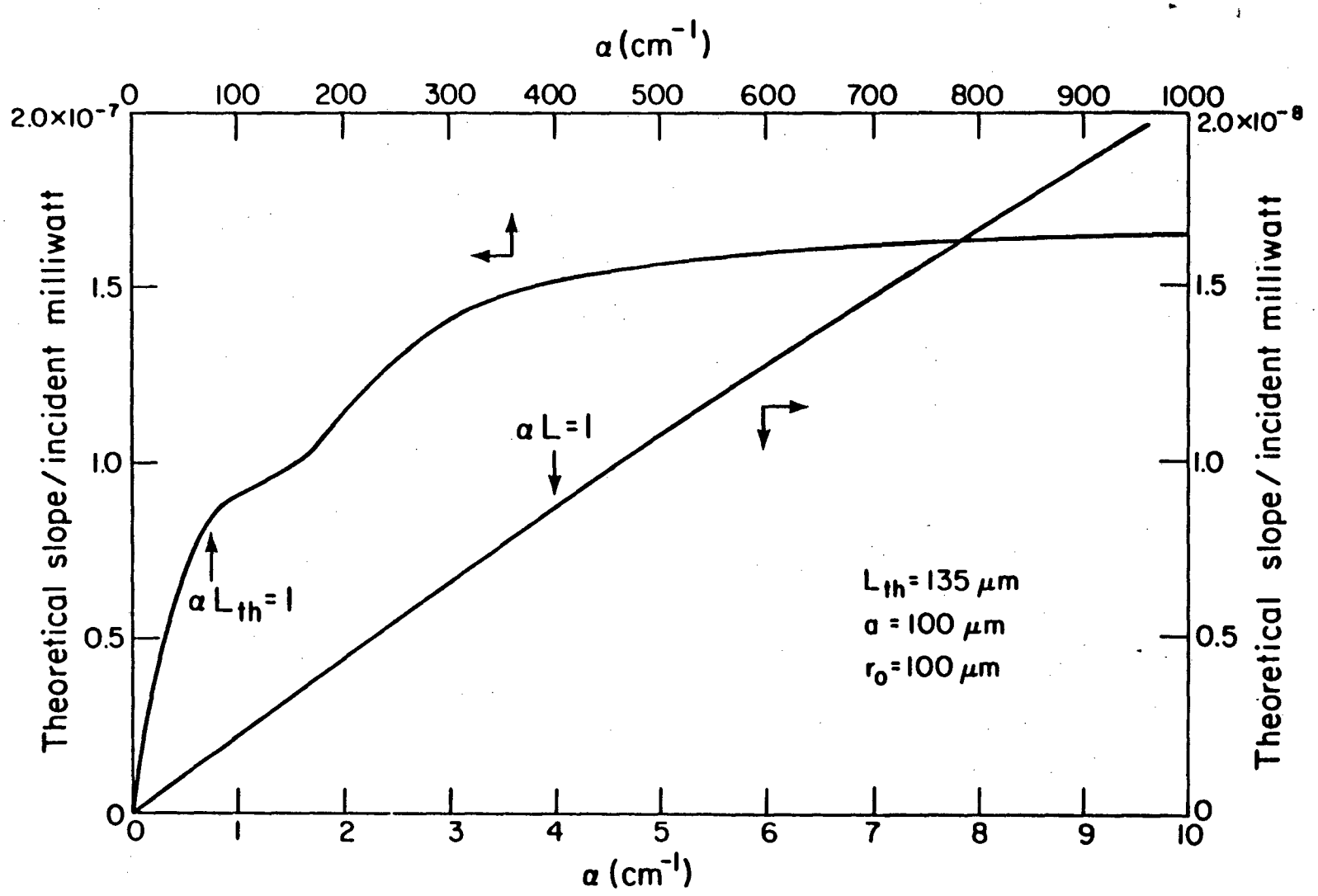

Figure 4

XBL 831 - 18

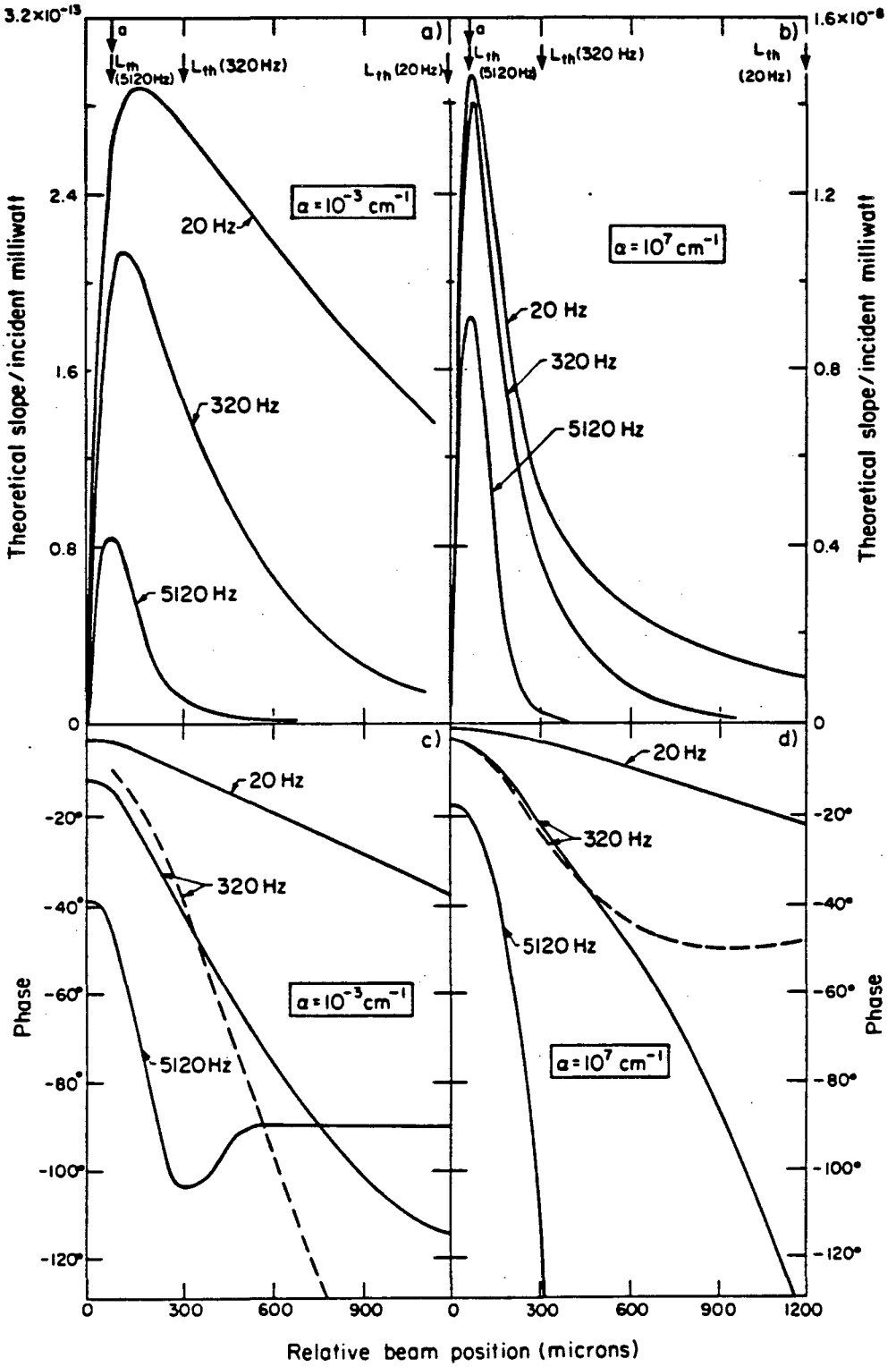
3.2×10⁻¹³
1.6×10⁻⁸
a)
b)
c)
d)
a
L_m (5120Hz)
L_{th} (320Hz)
L_{th} (20Hz)
L_{th} (5120Hz)
L_{th} (20Hz)
$\alpha = 10^{-3}$ cm^{-1}
$\alpha = 10^{7}$ cm^{-1}
20 Hz
320 Hz
5120 Hz
Theoretical slope/incident milliwatt
Phase
Relative beam position (microns)
0
300
600
900
1200
XBL 831 - 17

Figure 5

This report was done with support from the Department of Energy. Any conclusions or opinions expressed in this report represent solely those of the author(s) and not necessarily those of The Regents of the University of California, the Lawrence Berkeley Laboratory or the Department of Energy.

Reference to a company or product name does not imply approval or recommendation of the product by the University of California or the U.S. Department of Energy to the exclusion of others that may be suitable.

TECHNICAL INFORMATION DEPARTMENT
LAWRENCE BERKELEY LABORATORY
UNIVERSITY OF CALIFORNIA
BERKELEY, CALIFORNIA 94720